

March 1, 2019

Dear James Roberts,

We have responded below to your specific comments regarding the supplement to our manuscript, “pH-Dependent production of molecular chlorine, bromine, and iodine from frozen saline surfaces,” submitted to *Atmospheric Chemistry and Physics*. We thank you for your careful attention to this section, and we feel we have successfully addressed and clarified your questions, as indicated below (your comments in black, **our responses in blue**). We have also included in this document the revised Supplement with changes **highlighted in yellow**. We hope you find the manuscript is now complete and in publishable form.

Sincerely,

John W. Halfacre

I think you have answered all the reviewers' issues. I just have a few of my own.

Lines 15-20 in the Supplemental need some explanation and the first rate equation needs some work. Since you are using  $d[X_2]/dt$ , you are essentially assuming the  $OH + Cl^-$  is the rate limiting step to forming  $X_2$ . This needs to be explicitly stated here.

This passage has been clarified to indicate we are comparing the relative rates with which  $OH$  directly reacts with either the halides, or the buffer constituents ( $HSO_4^-$  or acetic acid) (lines 20-21). We have additionally clarified by altering “ $d[X_2]/dt$ ” to “ $d[X^-]/dt$ ” (lines 22-23).

Also, I don't understand  $d[SO_4]/dt$ . Shouldn't it be  $d[HSO_4^-]$ ? and doesn't this also assume that  $OH + HSO_4^-$  is the rate limiting step here? This should also be stated here.

You are correct, and we have adjusted the equation (line 22). We have additionally clarified that we are comparing competition between the direct reactions of  $X^-$  and buffer constituents ( $HSO_4^-$  and acetic acid) with  $OH$ , and not the  $X_2$  rate of formation (lines 20-21).

## 1 2. Methods

### 2 2.1 Materials

3 Acetic acid/acetate and bisulfate/sulfate buffer concentrations were 20 mM (10 mM of each acid and  
4 conjugate base). This concentration was chosen as a compromise between using as little buffer as possible and enough  
5 buffer to ensure adequate buffering ability, as buffer capacity rapidly decreases as constituent species concentrations  
6 approach the acid  $K_a$  value. The halide concentrations from our salt water solutions were  $\text{Cl}^-$  500mM,  $\text{Br}^-$  0.72mM,  
7 and  $\text{I}^-$   $1.9 \times 10^{-3}$  mM.

8 Given that the buffer concentration is comparable to or exceeds halide ion concentrations, there is a question  
9 of whether buffer composition may change over time due to the volatility of acetic acid (Henry's Law constant of 400  
10 M/atm), or because of buffer-constituent reactions with  $\text{OH}^\cdot$  (concentration of 100 mM) that may compete with  
11 reactions between  $\text{OH}^\cdot$  and halides. Here we present these potential reactions, associated rate constants, and calculate  
12 the potential for artifacts due to the presence of the buffer.



20 Using these aqueous rate constants and the pre-freezing concentrations of species (above and in main text Sect. 2.1),  
21 we find the following relative rates of  $\text{OH}^\cdot$  reactions with halides, compared to  $\text{OH}^\cdot$  reactions with buffer constituents:

22 
$$\frac{\frac{d[\text{X}^-]}{dt}}{\frac{d[\text{HSO}_4^-]}{dt}} = 3.6 \times 10^5, 1.7 \times 10^3, \text{ and } 4.4 \text{ for } \text{Cl}^-, \text{ Br}^-, \text{ and } \text{I}^-, \text{ respectively.}$$

23 
$$\frac{\frac{d[\text{X}^-]}{dt}}{\frac{d[\text{CH}_3\text{CO}_2\text{H}]}{dt}} = 1.8 \times 10^4, 8.6 \times 10^1, 2.3 \times 10^{-1} \text{ for } \text{Cl}^-, \text{ Br}^-, \text{ and } \text{I}^-, \text{ respectively.}$$

24 It is clear based on these relative rates of production that, assuming  $\text{OH}^\cdot + \text{HSO}_4^-$  is rate limiting, sulfate radical  
25 production would contribute only minorly to  $\text{Br}^-$  and  $\text{Cl}^-$  oxidation in our experiments, i.e., less than 0.1% of that from  
26  $\text{OH}^\cdot$ -halide oxidation. No analogous rate constant could be found for  $\text{I}^-$  reaction with the sulfate radical anion, and so

27 it is unclear the extent to which I<sup>-</sup> oxidation (and subsequent I<sub>2</sub> formation) may be impacted by formation of the sulfate  
28 radical. The oxidation of acetic acid has no impact on our experiments to our knowledge. While it might decrease  
29 the OH radical concentration, this would not impact our study of the relative rates of halide oxidation by OH. This is  
30 further supported by the fact that the pH measurements before and after experiments were statistically identical  
31 (indicating no significant depletion of either buffer species throughout the experiment, and consequently, no  
32 significant depletion of OH by reactions with either buffer species).

33

## 34 2.2 Flow tube

35 Reaction photochemistry was achieved using six UVA-340 solar simulator lamps (Q-Labs, 295 – 400 nm  
36 with maximum wattage at 340 nm, irradiance spectrum in Fig. S1). These lamps were installed in the experiment box  
37 (two on each side, except bottom). Each side was lined with reflective Mylar sheets to evenly irradiate the flow tube  
38 when the lamps were powered.

39

## 40 2.3 CIMS

41 Experiments utilizing the bisulfate/sulfate buffer (IO3-5, IO8, SW3-5, SW8, and CL1) sometimes exhibited  
42 cyclical CIMS signal changes for Br<sub>2</sub> (*m/z* 285, 287, 291), IBr (*m/z* 333, 335) with no attributable cause. These signal  
43 changes occurred seemingly at random and to varying extents. In Fig. S2a, Experiment IO4 (pH = 1.7, includes H<sub>2</sub>O<sub>2</sub>)  
44 demonstrates the most extreme example of this behaviour that almost appears to affect the analysis. First at t = -3, the  
45 Br<sub>2</sub> rises briefly before falling. Then at t=2, the Br<sub>2</sub> signal begins to resemble a sine wave. All data beyond t=2 is not  
46 considered for this specific experiment. In Fig S2b, the effect during Experiment SW5 (pH = 1.7, includes H<sub>2</sub>O<sub>2</sub>) is  
47 more muted, beginning at approximately t = -6 for IBr and Br<sub>2</sub>. As represented by these figures, this behaviour being  
48 farther away from our periods of integration is typical of the remaining experiments. Because these signal changes  
49 occurred outside of the experimental periods analyzed (i.e., before irradiation, and after O<sub>3</sub> had been active for one  
50 hour), they are therefore not believed to affect our results and their interpretation.

51

## 52 **3 Results and Discussion**

### 53 **3.1 Dark reaction production of I<sub>2</sub>**

54 In cases without OH precursors at pH < 2, significant photochemical I<sub>2</sub> production still occurs (integrated  
55 production of 14 ± 10 nmol for IO8, and 6.0 ± 2.0 nmol for SW8), while Br<sub>2</sub> and Cl<sub>2</sub> concentrations remain below  
56 limits of detection (consistent with Abbatt et al., (2010), in which no Br<sub>2</sub> was observed without an OH-precursor)  
57 (Table 2, main text). This production likely stems from the mechanisms outlined by Kim et al. (2016) (R13-14, R10-  
58 R12), discussed in the Sect. 1. As discussed in Sect. 3.1, H<sub>2</sub>O<sub>2</sub> or NO<sub>2</sub><sup>-</sup> can react directly with I<sup>-</sup>, thereby reducing the  
59 available [I<sup>-</sup>] for photochemical OH oxidation when pH < 2. When H<sub>2</sub>O<sub>2</sub> was the oxidant, integrated I<sub>2</sub> production  
60 amounts were found to be ≤ 0.82 nmol (IO4, IO5, and SW5), likely due to this initial dark depletion. When instead  
61 NO<sub>2</sub><sup>-</sup> is used (as in IO3 and SW3), initial amounts of I<sub>2</sub> on flowtube connection to CIMS were less than when H<sub>2</sub>O<sub>2</sub>  
62 was used (Table S1, Fig. S3). To estimate how much I<sup>-</sup> may have been lost from our frozen sample by these dark  
63 mechanisms, we convert the integrated I<sub>2</sub> production amounts from Table S1 to I<sup>-</sup> (by multiplying by 2) and subtract  
64 from the maximum possible moles of I<sup>-</sup> in our samples (0.0800 L \* 1.6 x 10<sup>-6</sup> M = 1.28 x 10<sup>-7</sup> moles I<sup>-</sup>). For the  
65 samples that use hydrogen peroxide, as little as 36–91% of I<sup>-</sup> is available for reaction, while 94-97% remain when  
66 using NO<sub>2</sub><sup>-</sup>. However, it is certain that not all of the I<sub>2</sub> produced by this mechanism went into the CIMS by the nature  
67 of having to break the flow tube seal in order to connect it to the CIMS. Therefore, these are only estimates that could  
68 be affected by the length of time the tube is open to the environment and not connected to the CIMS, or sealed shut.  
69

### 70 **3.2 Hydroxyl radical-induced halogen production**

#### 71 **3.2.1 pH ≈ 4.7**

72 Considering the values of I<sub>2</sub> production from Table 2 (main text), IO2, appears to have produced ~10 times  
73 less I<sub>2</sub> based on the chosen period of integration. It was noted that I<sub>2</sub> appeared to already be present within the flow  
74 tube on connecting the flow tube to the CIMS (Fig. S4). The integrated sum of I<sub>2</sub> released on connection of the flow  
75 tube to the CIMS until stabilization was 0.8 (± 0.1) nmol, corresponding to approximately 0.5% of the total 152 nmol  
76 I<sup>-</sup> available for reaction from the Instant Ocean solution (Table S1). This production could possibly be induced by the  
77 dark reactions described in Sect. 3.1. However, the experiment otherwise eventually produces the same qualitative  
78 features as the other three experiments after light activation (Fig. S4). If instead the limits of integration are chosen

79 starting when the I<sub>2</sub> signal begins rising (i.e., during a period that qualitatively resembles the other experiments), the  
80 integrated I<sub>2</sub> production amounts ( $1.1 \pm 0.6$  nmol) more closely approaches analogous experiments (IO1, SW1, SW2).  
81 The apparent photochemical integrated Br<sub>2</sub> sum of  $0.034 \pm 0.003$  nmol (Table 2) represents a real signal just above  
82 the limit of detection ( $1.8 \pm 0.4$  pmol mol<sup>-1</sup>), but this baseline signal does not change on addition of light (Fig. 3a). In  
83 addition, the integration method used likely interpolated missing data for time periods in which incorrect isotope ratios  
84 between *m/z* 285 and 287 were observed, thereby overestimating the integrated yield. This signal remains below  
85 limits of quantitation and should not be considered further. Cl<sub>2</sub> concentrations remained below limits of detection for  
86 experiment IO2.

87 In most cases, it was also found that extending limits of integration beyond 1 h after addition of O<sub>3</sub> did not  
88 produce I<sub>2</sub> in amounts that exhausted the supply of I<sup>-</sup>. In an example experiment (IO2, Fig. S5), the limits of integration  
89 were extended to *t* = 15 hours after the initiation of lights. While the signal appeared to stabilize below the I<sub>2</sub> LOD of  
90 9 pmol mol<sup>-1</sup>, the calculated I<sub>2</sub> production amount of 70 nmol for this extended integration period only accounts for  
91 46% of the 152 total nmol of I<sup>-</sup> available. When repeated for the other experiments at pH = 4.7, it is found that at least  
92 16% of the original I<sup>-</sup> remains unreacted after similarly extended limits of integration. This suggests that all of the I<sup>-</sup>  
93 in our frozen samples may not be completely excluded to the disordered interface, and may exist within the ice bulk  
94 or inaccessible brine channels throughout the ice, and that differences in integration production amounts can originate  
95 from differences in I<sup>-</sup> distribution during freezing (Bartels-Rausch et al., 2014; Malley et al., 2018).

### 96 3.2.2 pH ≤ 2

97 At low pH (~2), and with H<sub>2</sub>O<sub>2</sub> as our OH precursor, we noted a large outflux of I<sub>2</sub> on connecting the flow  
98 tube to the CIMS. Br<sub>2</sub> production was readily observed in the presence of light, and enhanced when the samples were  
99 exposed to O<sub>3</sub>, as in Fig 2b. However, experiment SW3 (Fig. S5), which was performed with NO<sub>2</sub><sup>-</sup> as the hydroxyl  
100 radical precursor, exhibited photochemical I<sub>2</sub> production on the introduction of radiation. Only after the introduction  
101 of O<sub>3</sub> was Br<sub>2</sub> observed (under proper isotope ratios).

102

### 103 3.3 Effects of O<sub>3</sub> on halogen production

104 As discussed in the main text, HOX compounds were observed when O<sub>3</sub> was added to the flow tube. With  
105 regard to the extent to which it affects our observed signal, we believe volatile organic compounds, such as aldehydes

106 and ketones, that may form gas phase HX could originate from our cylinder of zero air. However, we believe this  
107 source would be effectively scrubbed by our activated charcoal trap (Fig. 1), mitigating any gas phase production of  
108 HX. There also exists organic matter in the condensed phase, averaging 70 mg/L in each Instant Ocean sample (Sect.  
109 2 of the main text). This carbon-matter is presumably uncharged and would freeze throughout the formed ice (i.e., no  
110 freeze concentration effect), therefore making only a small fraction of the total carbon available at the frozen surface  
111 for reaction.

112 If any of this solution-based carbon were involved in making HX, it would be expected that the SW and IO  
113 experiments produce different amounts of IOHX<sup>-</sup>, given that the SW experiments were found to average ~5 mg/L of  
114 dissolved organic matter. However, there is no difference in the signal changes between corresponding SW and IO  
115 experiments (Figs. 3-4, S6). Therefore, we believe the primary source of IOHX<sup>-</sup> in the CIMS is, indeed, HOX formed  
116 in the flow tube.

117

118

## 119 **References**

- 120 Abbatt, J., Oldridge, N., Symington, A., Chukalovskiy, V., McWhinney, R. D., Sjostedt, S. and Cox, R. A.: Release  
121 of Gas-Phase Halogens by Photolytic Generation of OH in Frozen Halide–Nitrate Solutions: An Active Halogen  
122 Formation Mechanism?, *J. Phys. Chem. A*, 114(23), 6527–6533, doi:10.1021/jp102072t, 2010.
- 123 Bartels-Rausch, T., Jacobi, H.-W., Kahan, T. F., Thomas, J. L., Thomson, E. S., Abbatt, J. P. D., Ammann, M.,  
124 Blackford, J. R., Bluhm, H., Boxe, C., Domine, F., Frey, M. M., Gladich, I., Guzmán, M. I., Heger, D., Huthwelker,  
125 T., Klán, P., Kuhs, W. F., Kuo, M. H., Maus, S., Moussa, S. G., McNeill, V. F., Newberg, J. T., Pettersson, J. B. C.,  
126 Roeselová, M. and Sodeau, J. R.: A review of air–ice chemical and physical interactions (AICI): liquids, quasi-liquids,  
127 and solids in snow, *Atmos Chem Phys*, 14(3), 1587–1633, doi:10.5194/acp-14-1587-2014, 2014.
- 128 Buxton, G. V., Greenstock, C. L., Helman, W. P. and Ross, A. B.: Critical Review of rate constants for reactions of  
129 hydrated electrons, hydrogen atoms and hydroxyl radicals ( $\cdot\text{OH}/\cdot\text{O}^-$  in Aqueous Solution, *J. Phys. Chem. Ref. Data*,  
130 17(2), 513–886, doi:10.1063/1.555805, 1988.
- 131 Grigor'ev, A. E., Makarov, I. E. and Pikaev, A. K.: Formation of  $\text{Cl}_2^-$  in the bulk of solution during radiolysis of  
132 concentrated aqueous solutions of chlorides, *Khimiya Vysok. Ehnergij*, 21(2), 123–126, 1987.
- 133 Jiang, P.-Y., Katsumura, Y., Nagaishi, R., Domae, M., Ishikawa, K., Ishigure, K. and Yoshida, Y.: Pulse radiolysis  
134 study of concentrated sulfuric acid solutions. Formation mechanism, yield and reactivity of sulfate radicals, *J. Chem.*  
135 *Soc. Faraday Trans.*, 88(12), 1653–1658, doi:10.1039/FT9928801653, 1992.
- 136 Malley, P. P. A., Chakraborty, S. and Kahan, T. F.: Physical Characterization of Frozen Saltwater Solutions Using  
137 Raman Microscopy, *ACS Earth Space Chem.*, doi:10.1021/acsearthspacechem.8b00045, 2018.

138 Padmaja, S., Neta, P. and Huie, R. E.: Rate constants for some reactions of inorganic radicals with inorganic ions.  
139 Temperature and solvent dependence, *Int. J. Chem. Kinet.*, 25(6), 445–455, doi:10.1002/kin.550250604, 1993.  
140 Redpath, J. L. and Willson, R. L.: Chain Reactions and Radiosensitization: Model Enzyme Studies, *Int. J. Radiat.*  
141 *Biol. Relat. Stud. Phys. Chem. Med.*, 27(4), 389–398, doi:10.1080/09553007514550361, 1975.  
142 Thomas, J. K.: Rates of reaction of the hydroxyl radical, *Trans. Faraday Soc.*, 61(0), 702–707,  
143 doi:10.1039/TF9656100702, 1965.  
144 Zehavi, D. and Rabani, J.: Oxidation of aqueous bromide ions by hydroxyl radicals. Pulse radiolytic investigation, *J.*  
145 *Phys. Chem.*, 76(3), 312–319, doi:10.1021/j100647a006, 1972.

146

147

148

149

150

151

152

153

154

155

156

157

158

159

160

161 **Tables**

162 Table S1: Integrated I<sub>2</sub> production amounts prior to irradiation or addition of O<sub>3</sub> from low pH experiments  
163 involving samples with an OH precursor. The period of integration was chosen to be immediately after  
164 connection of flow tube to the CIMS until sample was irradiated. Average LODs for I<sub>2</sub> across experiments  
165 was  $9 \pm 2$  pmol mol<sup>-1</sup>. “IO#” represents samples composed of Instant Ocean, and “SW#” represents  
166 “saltwater” samples, composed of reagent salts.

167

Experiment	Oxidant	pH	I <sub>2</sub> produced (nmol)	Integration time (hours)	Estimated Percent of I <sup>-</sup> remaining for reaction
IO3	NO <sub>2</sub> <sup>-</sup>	2.0	4.0(±0.1)	0.55	93.7
SW4	NO <sub>2</sub> <sup>-</sup>	2.2	2.5(±0.1)	0.43	96.1
SW3	NO <sub>2</sub> <sup>-</sup>	1.8	2.0(±0.1)	0.83	96.8
IO4	H <sub>2</sub> O <sub>2</sub>	1.7	41(±14)	7.28	36.2
IO5	H <sub>2</sub> O <sub>2</sub>	1.7	5.7(±1.9)	2.92	91.1
SW5	H <sub>2</sub> O <sub>2</sub>	1.8	41(±14)	4.95	35.5

168

169



170

171 Table S2: Integrated I<sub>2</sub> produced from pH = 4.7 experiments involving samples with an OH precursor. The  
172 period of integration begins at sample irradiation and extends past the limits of analysis used in the main  
173 text. Average LODs for I<sub>2</sub> across experiments was  $9 \pm 2$  pmol mol<sup>-1</sup>. “IO#” represents samples composed  
174 of Instant Ocean, and “SW#” represents “saltwater” samples, composed of reagent salts.

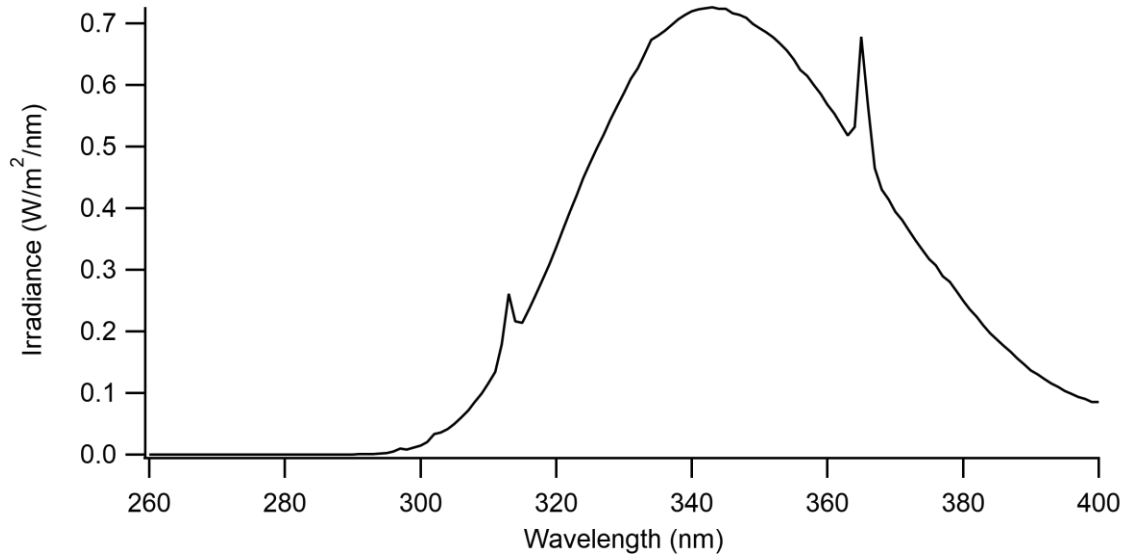
175

Experiment	Oxidant	pH	I <sub>2</sub> produced (nmol)	Integration time (hours)	Estimated Percent of I <sup>-</sup> remaining for reaction
IO1	H <sub>2</sub> O <sub>2</sub>	4.7	31(±10)	30	59
IO2	H <sub>2</sub> O <sub>2</sub>	4.7	35(±20)	15	54
SW1	H <sub>2</sub> O <sub>2</sub>	4.7	63(±23)	23	17
SW2	H <sub>2</sub> O <sub>2</sub>	4.5	63(±20)	17	16

176

177

178

180 **Figures**

181

182 Figure S1: Irradiance spectrum for the Q-Lab UVA 340 Lamps, reproduced with permission from Q-Lab  
183 Corporation Technical Bulletin LU-8052 – “SPD for QUV UVA-340.”

184

185

186

187

188

189

190

191

192

193

194

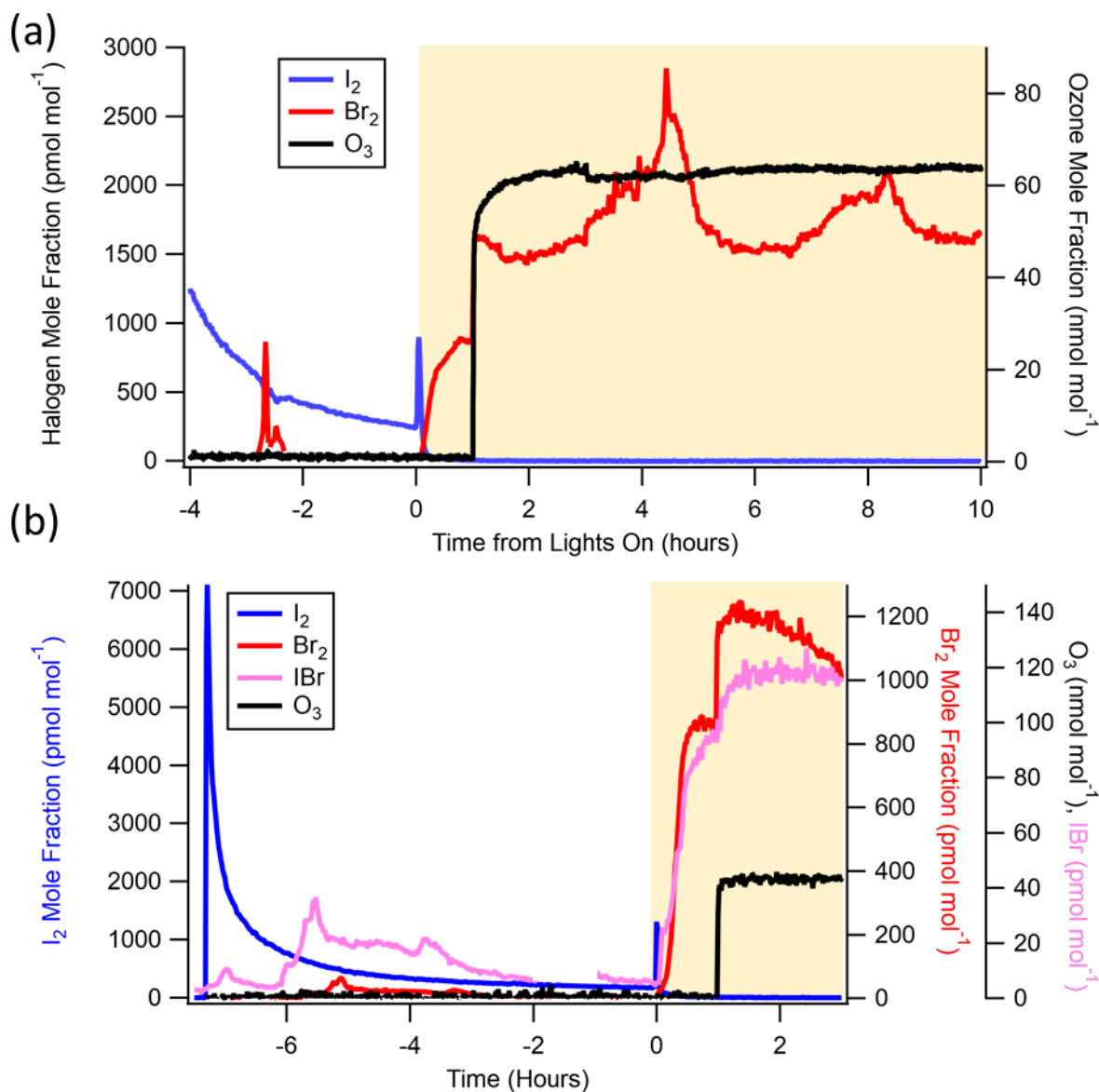
195

196

197

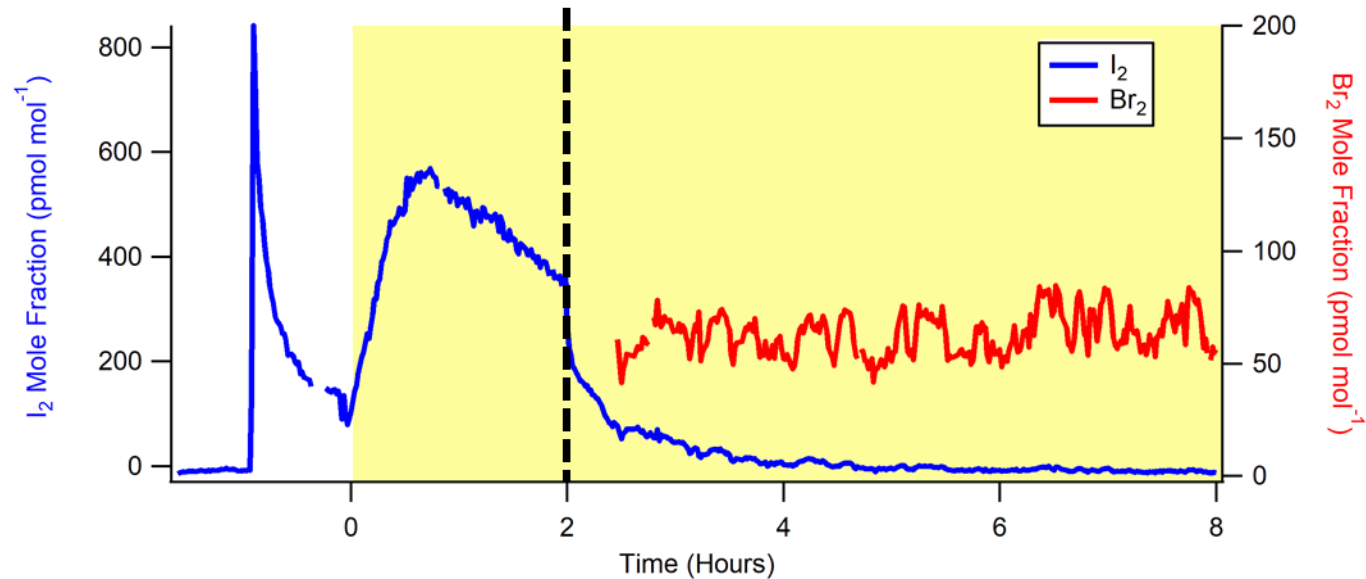
198

199



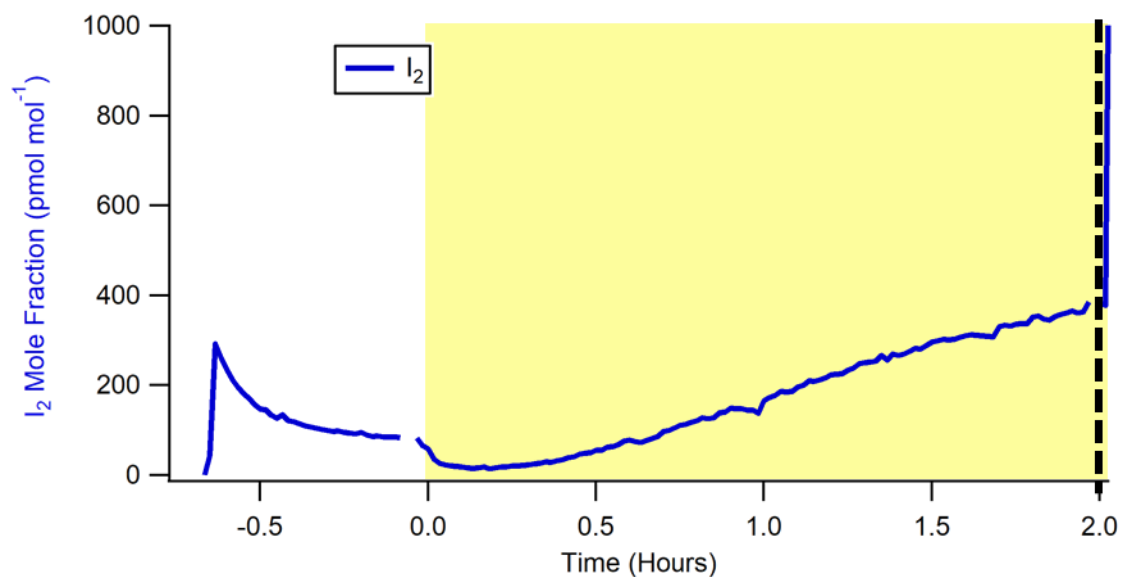
200  
 201 Figure S2: a) Experiment IO4 ( $pH < 2$ , includes  $H_2O_2$ ) time series demonstrating cyclical increases in signal  
 202  $Br_2$  signals, especially at  $t = -3$  and beginning again at  $t = 2$ . Period of analysis in main text includes  $t = 0$   
 203 until  $t = 2$ . b) Experiment SW5 ( $pH < 2$ , includes  $H_2O_2$ ) time series demonstrating cyclical signals for  $IBr$   
 204 and  $Br_2$ , beginning predominately at  $t = -6$  until shortly before  $t = 0$ .

205  
 206  
 207  
 208  
 209



210  
 211 Figure S3: Experiment SW3, using synthetic seawater at pH = 1.8, in which  $\text{NO}_2^-$  acted as our hydroxyl  
 212 radical precursor. Ozone was introduced at hour two (indicated by dashed vertical line), coincident with  
 213 the  $\text{I}_2$  concentration decrease.  $\text{Br}_2$  data filtered based on correctness of isotope ratios between  $m/z$  285 and  
 214 287 (IBrBr).  
 215

216

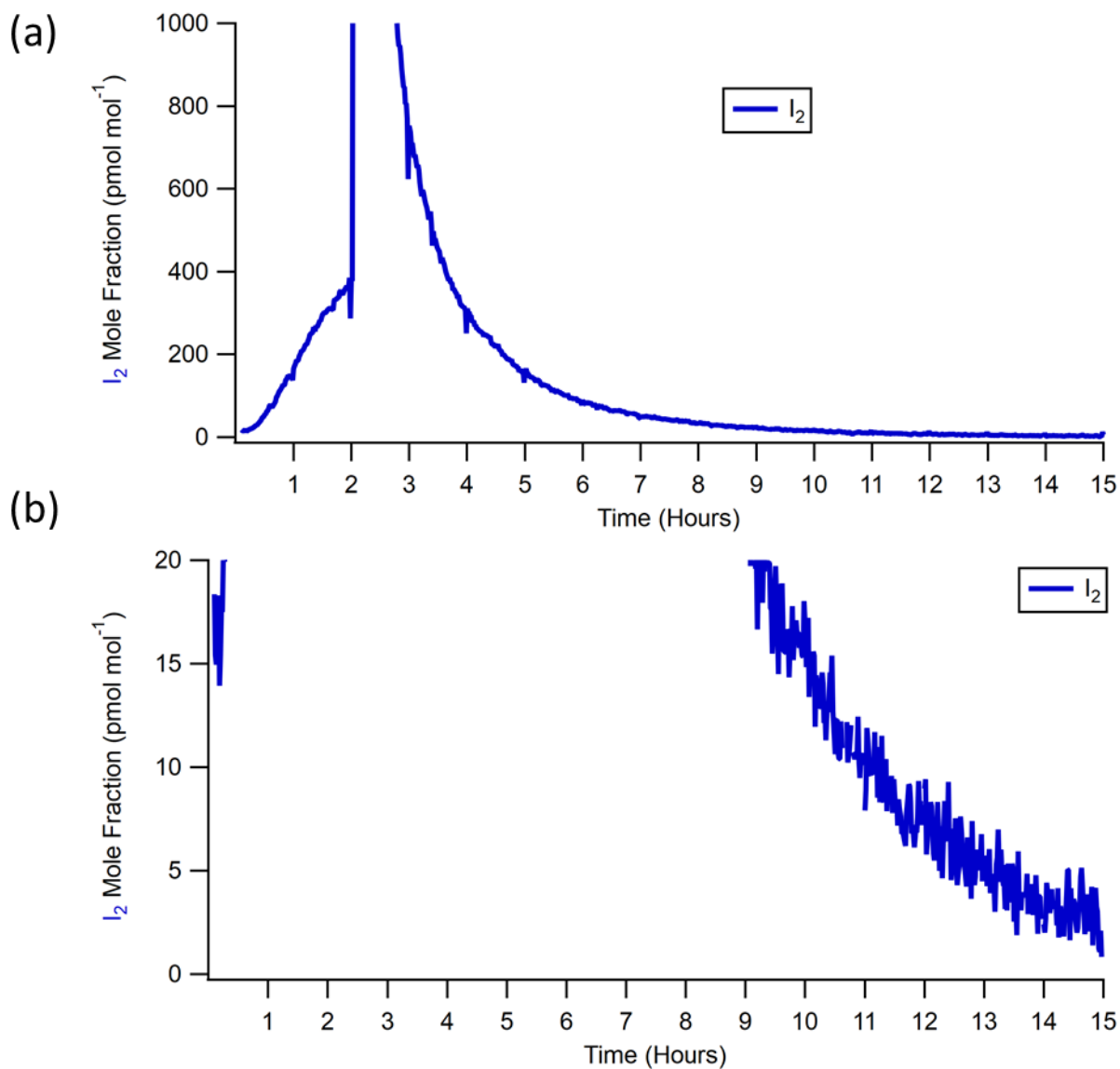


217

218

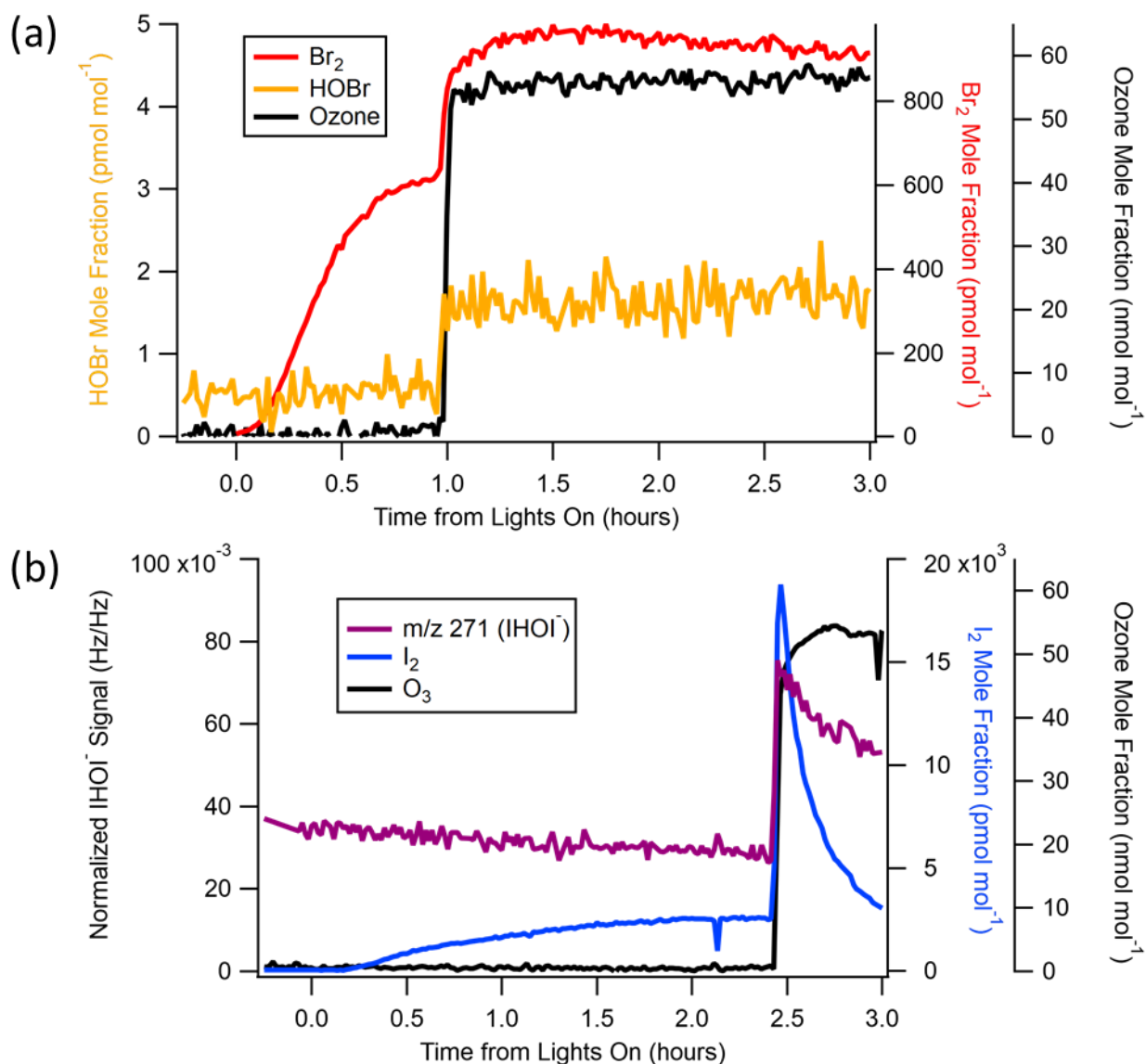
219 Figure S4: Experimental timeseries for experiment IO2. The key difference between this experiment and  
220 others at pH ~4.68 is that there was some initial I<sub>2</sub> present when the flow tube was connected to the CIMS.  
221 On activating the lights, these concentrations lowered, before ultimately rising due to OH-induced I<sub>2</sub>  
222 production. Beginning the integration when the signal begins rising leads to similar production values as  
223 those experiments without this initial I<sub>2</sub> present. Vertical dashed line represents when O<sub>3</sub> was introduced  
224 to the system.

225



226  
 227  
 228  
 229  
 230  
 231  
 232  
 233  
 234

Figure S5: Iodine time series from experiment IO2, using Instant Ocean at pH = 4.7, in which H<sub>2</sub>O<sub>2</sub> acted as our hydroxyl radical precursor. The x-axis begins on light introduction to the flow tube, while ozone was introduced at hour two as indicated by the sudden increase in signal. (a) The time series signal rapidly increases at t=2 coincident with the addition of 60 nmol mol<sup>-1</sup> of O<sub>3</sub>, and then returns to baseline by hour 13. (b) Zoomed in version of the same plot



235  
 236 Figure S6: a) Experiment IO5, using Instant Ocean at pH = 1.7, in which  $\text{H}_2\text{O}_2$  acted as our hydroxyl radical  
 237 precursor (analogous to SW5, Fig. 4). Comparison of  $\text{Br}_2$  mole fractions to HOBr. Note that the HOBr  
 238 signal should be used only for qualitative purposes as its identity could not be confirmed using isotopic  
 239 ratios with  $m/z$  223 due to its relatively large background signal.  $\text{Br}_2$  data filtered based on correctness of  
 240 isotope ratios between  $m/z$  285 and 287 ( $\text{IBrBr}^-$ ). b) Experiment SW2 (analogous to IO2, Fig. 3) showing  
 241 effect of  $\text{O}_3$  on  $\text{I}_2$  and HOI.  
 242  
 243